Available online at www.sciencedirect.com

ScienceDirect

Geochimica et Cosmochimica Acta 222 (2018) 117–129

Geochimica et Cosmochimica Acta

www.elsevier.com/locate/gca

Theoretical isotopic fractionation between structural boron in carbonates and aqueous boric acid and borate ion

Etienne Balan [a,*], Johanna Noireaux [b,1], Vasileios Mavromatis [c], Giuseppe D. Saldi [c], Valérie Montouillout [d], Marc Blanchard [c], Fabio Pietrucci [a], Christel Gervais [e], James R. Rustad [f], Jacques Schott [c], Jérôme Gaillardet [b,g]

[a] *Sorbonne Universités – Institut de Minéralogie, de Physique des Matériaux et de Cosmochimie (IMPMC), UPMC Université Paris 6, UMR CNRS 7590, UMR IRD 206, MNHN, 4 place Jussieu, 75252 Paris cedex 05, France*

[b] *Institut de Physique du Globe de Paris, Sorbonne Paris Cité, Université Paris Diderot, CNRS, F-75005 Paris, France*

[c] *Géosciences Environnement Toulouse, Observatoire Midi-Pyrénées, CNRS-Université de Toulouse, 14, avenue Edouard Belin, 31400 Toulouse, France*

[d] *CEMHTI CNRS UPR3079, Université d'Orléans, 45071 Orléans cedex 1, France*

[e] *Sorbonne Universités – Laboratoire de Chimie de la Matière Condensée de Paris (LCMCP), UPMC Université Paris 6, UMR CNRS 7574, 4 place Jussieu, 75252 Paris cedex 05, France*

[f] *Office of Basic Energy Sciences, SC-22.1/Germantown Building, U.S. Department of Energy, 1000 Independence Avenue, SW, Washington, D.C. 20585-1290, United States*

[g] *Institut Universitaire de France, France*

Received 11 April 2017; accepted in revised form 15 October 2017; available online 25 October 2017

Abstract

The $^{11}B/^{10}B$ ratio in calcite and aragonite is an important proxy of oceanic water pH. However, the physico-chemical mechanisms underpinning this approach are still poorly known. In the present study, we theoretically determine the equilibrium isotopic fractionation properties of structural boron species in calcium carbonates, BO_3^{3-}, $BO_2(OH)^{2-}$ and $B(OH)_4^-$ anions substituted for carbonate groups, as well as those of $B(OH)_4^-$ and $B(OH)_3$ species in vacuum. Significant variability of equilibrium isotopic fractionation properties is observed among these structural species which is related to their contrasted coordination state, B—O bond lengths and atomic-scale environment. The isotopic composition of structural boron does not only depend on its coordination number but also on its medium range environment, i.e. farther than its first coordination shell. The isotopic fractionation between aqueous species and their counterparts in vacuum are assessed using previous investigations based on similar quantum-mechanical modeling approaches. At 300 K, the equilibrium isotope composition of structural trigonal species is 7–15‰ lighter than that of aqueous boric acid molecules, whereas substituted tetrahedral borate ions are heavier than their aqueous counterparts by 10–13‰. Although significant uncertainties are known to affect the theoretical prediction of fractionation factors between solids and solutions, the usually assumed lack of isotopic fractionation during borate incorporation in carbonates is challenged by these theoretical results. The present theoretical equilibrium fractionation factors between structural boron and aqueous species differ from those inferred from experiments which may indicate that isotopic equilibrium, unlike chemical equilibrium, was not reached in most experiments. Further research into the isotopic fractionation processes at the interface between calcium carbonates and aqueous solution as well as long duration experiments aimed at investigating the kinetics of equilibration of boron environment and isotopic composition are therefore

* Corresponding author at: Institut de Minéralogie, Physique des Matériaux et Cosmochimie, Case 115, 4 place Jussieu, 75252 Paris Cedex 05, France. Fax: +33 1 44 27 37 85.

E-mail address: Etienne.Balan@upmc.fr (E. Balan).

[1] Now at LNE, 1, rue Gaston Boissier, 75015 Paris, France.

https://doi.org/10.1016/j.gca.2017.10.017

required to refine our understanding of boron coprecipitation in carbonates and thus the theory behind the use of boron isotopes as an ocean pH proxy.

Keywords: Boron pH-proxy; Ab initio modeling; Theoretical isotopic fractionation factors; Calcium carbonates

1. INTRODUCTION

The isotopic composition of boron ($^{11}B/^{10}B$ ratio) in biogenic calcium carbonates is a key proxy of seawater pH which in turn depends on the secular variations of atmospheric CO_2 concentrations (Vengosh et al., 1991; Hemming and Hanson, 1992; Spivack et al., 1993). A major assumption sustaining this approach is that only one species, the tetrahedral borate ion, $B(OH)_4^-$, is incorporated in the crystal without isotopic fractionation during its growth from aqueous solution whereas isotopically heavier trigonal boric acid molecules, $B(OH)_3$, are not incorporated. Accordingly, the isotopic composition of carbonates should simply be controlled by the pH-dependent borate/boric acid ratio of the solution (Hemming and Hanson, 1992).

Aragonite samples obtained from inorganic precipitation experiments at low supersaturation conditions (Noireaux et al., 2015) fit with this model. Their isotopic composition reflects that of aqueous borate, and boron in the solid phase predominantly occurs in a tetrahedral environment. In contrast, biogenic or inorganic natural aragonite samples may present significant departure from the model (e.g., Stewart et al., 2016; Zhang et al., 2017). Concerning calcite, the samples often display a significant proportion of trigonal boron (Sen et al., 1994; Klochko et al., 2009; Branson et al., 2015; Mavromatis et al., 2015). Their isotopic composition and the observed boron speciation can be reconciled through a mechanism involving a recoordination of the borate ion from tetrahedral to trigonal coordination in the surface layer of growing carbonate crystals, leaving unaffected its boron isotopic composition (Hemming and Hanson, 1992; Hemming et al., 1998; Branson et al., 2015). Fixation of boron on specific sites of the calcite surface and associated non-equilibrium processes have been revealed by several studies (Hemming et al., 1998; Hobbs and Reardon, 1999; Ruiz-Agudo et al., 2012). A dependence of boron incorporation on the calcite growth rate has also been pointed out (Gabitov et al., 2014; Mavromatis et al., 2015; Noireaux et al., 2015; Uchikawa et al., 2015; Kaczmarek et al., 2016) suggesting that this process could be described using the growth entrapment model (Watson, 2004) or the more recently proposed surface-kinetic model (DePaolo, 2011). However, these parameterized models do not perfectly account for the complex mechanisms of trace element incorporation in carbonates (Mavromatis et al., 2013; Watkins et al., 2017). Heavier than expected isotopic compositions of some samples also suggested incorporation of heavier boric acid molecules (Noireaux et al., 2015). Their incorporation likely involves a modification of the coordination sphere of boron to comply with electrostatic charge balance requirements (Hemming and Hanson, 1992; Uchikawa et al., 2015).

In the current models of boron incorporation in carbonates, isotopic fractionation between aqueous and structural boron species is usually assumed to be negligible, mostly because of the lack of available quantitative data. However, earlier measurements on boron species adsorbed on humic acids and oxide minerals (Lemarchand et al., 2005, 2007) as well as calculations on molecular species of boron (Liu and Tossell, 2005; Tossell, 2005, 2006) suggested potential fractionation effects related to distortions of the first coordination shell of boron. Recently, atomic-scale models of $BO_2(OH)^{2-}$ and $B(OH)_4^-$ anions substituted for carbonate groups have been shown to be consistent with NMR spectroscopic observations of trigonal and tetrahedral environments, respectively, confirming initial assumptions and shedding light on the most common speciation of boron in synthetic and natural calcium carbonates (Balan et al., 2016). In addition, quantum mechanical calculations can now be used to compute theoretical equilibrium isotopic fractionation factors in a predictive way, i.e. without introducing parameters adjusted on experiments (e.g. Rustad, 2016; Blanchard et al., 2017). These approaches can provide important insights in the equilibrium configuration and isotopic fractionation properties of the molecular species incorporated at trace concentration levels in minerals, such as CO_2 in pedogenic oxides (Rustad and Zarzycki, 2008). They have been also used to determine the isotopic fractionation factors between aqueous boron species (Liu and Tossell, 2005; Rustad and Bylaska, 2007; Rustad et al., 2010; Kowalski et al., 2013). Based on this modeling strategy and the previous theoretical studies of aqueous boron species, it is possible to determine the theoretical equilibrium isotopic fractionation factors between structural boron species and their aqueous counterparts, providing a theoretical basis to discuss potential isotopic fractionation effects during the incorporation of boron in inorganic calcium carbonates.

2. METHODS

The investigated models of boron-bearing calcium carbonates (Balan et al., 2016) are based on $2 \times 2 \times 2$ supercells of calcite (rhombohedral cell, 80 atoms) and aragonite (160 atoms). Benchmark calculations have also been performed on borate ion and boric acid in vacuum, here referred to as isolated boron species. To this purpose, a single molecule was inserted in a large cubic box with cell parameter $a = 15.87$ Å as in, e.g., Kowalski et al. (2013). For the borate ion, the electrostatic charge balance was ensured by a counter-charge homogeneously spread over the cell.

The theoretical properties of structural and isolated boron species were investigated within the density functional theory (DFT) framework, using periodic boundary conditions and the generalized gradient approximation (GGA) to the exchange-correlation functional as proposed by Perdew, Burke and Ernzerhof (PBE; Perdew et al., 1996). Calculations were performed using the QUANTUM ESPRESSO package (Giannozzi et al., 2009; http://www.quantum-espresso.org). The same pseudo-potentials and numerical parameters as in Balan et al. (2016) were used. The ionic cores were described by ultra-soft pseudopotentials from the GBRV library (Garrity et al., 2014). The electronic wave-functions and charge density were expanded using a finite basis sets of plane-waves with 40 and 200 Ry cutoffs, respectively, corresponding to a convergence of the total energy better than 1 mRy/atom. Structural relaxations have been performed using a 10^{-4} Ry per atomic unit convergence parameter for the forces on atoms.

Standard equilibrium isotopic fractionation is closely related to the change of vibrational energy levels induced by the isotopic mass variation. These temperature-dependent equilibrium properties of a system can be discussed in terms of reduced partition function ratios (RPFRs, "β-factors"), i.e. isotopic fractionation factors determined between the quantum system of interest and an ideal reference system whose behavior would be solely described by the laws of classical mechanics (Bigeleisen and Mayer, 1947; Richet et al., 1977). The isotopic fractionation coefficient between two substances a and b, referred to as $\alpha(a, b)$, is related to the RPFRs by:

$$\ln \alpha(a,b) = \ln \beta(a) - \ln \beta(b) \quad (1)$$

Although not directly accessible by experiments, the RPFRs of a given system can be computed from the harmonic vibrational frequencies using the expressions previously given by, e.g., Schauble et al. (2006) and Méheut et al. (2007):

$$\beta = \left[\prod_{i=1}^{3N} \prod_{\{q\}} \frac{\nu^*_{q,i}}{\nu_{q,i}} \times \frac{e^{-\frac{h\nu^*_{q,i}}{2kT}}}{1 - e^{-\frac{h\nu^*_{q,i}}{kT}}} \times \frac{1 - e^{-\frac{h\nu_{q,i}}{kT}}}{e^{-\frac{h\nu_{q,i}}{2kT}}} \right]^{\frac{1}{Nq^n}} \quad (2)$$

where $\nu_{q,i}$ and $\nu^*_{q,i}$ are the frequency of the vibrational mode defined by indexes i and wavevector q for the two isotopically distinct systems, N the total number of atoms per unit cell, Nq the number of wavevectors, n the number of isotopically exchanged sites (1 in the present study), h the Planck constant, k the Boltzmann constant, T the temperature. Eq. (2) uses the Teller-Redlich rule which ensures that a classical behavior of the system, corresponding to vanishing isotopic fractionation, is retrieved at high temperature. Only raw harmonic frequencies obtained using the linear response theory (Baroni et al., 2001) were used to compute the RPFRs using Eq. (2) as recommended by Liu et al. (2010). In periodic crystal structures, the dependence of vibrational frequencies on phonon wavevectors is related to the collective vibrational displacements of atoms belonging to different crystal cells. As the present study only considers isolated molecular species in vacuum or chemical defects in large super-cells, the harmonic frequencies were only calculated at the Brillouin zone center (Γ point). In addition, the localized mode approximation (Balan et al., 2014) was used for the structural species in crystalline hosts by restricting the computation to the dynamical matrix coefficients involving a displacement of the B, O and H

Table 1
Structural parameters of boron species in calcium carbonates and reduced partition function ratios (RPFRs) at 300 K.

B coordinence	Species	Model	B—O bond length (Å)	β (300 K)
Trigonal	Isolated	$B(OH)_3$	1.378	1.2196
	Calcite	BO_3^{3-}	1.388	1.1968
		$BO_2(OH)^{2-}$	1.345	1.1969
			1.350	
			O(H) 1.491	
	Aragonite	BO_3^{3-}	1.380	1.2056
			1.383 (x2)	
		$BO_2(OH)^{2-}$ (A)	1.343	1.2025
			1.350	
			O(H) 1.472	
		$BO_2(OH)^{2-}$ (B)	1.347	1.2006
			1.349	
			O(H) 1.472	
Tetragonal	Isolated	$B(OH)_4^-$	1.495	1.1741
	Calcite	$B(OH)_4^-$	O1 1.438	1.1901
			O3 1.477	
			O4 1.489	
			O2 1.510	
	Aragonite	$B(OH)_4^-$	O2 1.455	1.1871
			O1 1.476	
			O3 1.497	
			O4 1.497	

atoms belonging to the molecular anionic boron species. Compared with a full calculation on the tetragonal borate in calcite, RPFRs differ by less than 0.3‰ at 300 K. Note that this approximation requires that atoms not belonging to the molecular anionic cluster do not contribute to the eigenvectors of the partial dynamical matrices (a condition that can be ensured by setting their atomic mass to a very large value), otherwise more erratic results can be obtained as observed by Dupuis et al. (2015).

3. RESULTS

In the isolated molecules, the relaxed B—O bond lengths are 1.378 Å and 1.495 Å for $B(OH)_3$ and $B(OH)_4^-$, respectively (Table 1). Corresponding harmonic frequencies (Table S1) compare well with those previously computed using the GGA PBE (Rustad et al., 2010) and BLYP functionals (Zeebe, 2005; Kowalski et al., 2013) (Fig. S1). For tetrahedral borate, the sensitivity of vibrational frequencies to isotopic substitution (Fig. 1, Table S1) decreases in the order: anti-symmetric B—O stretching modes (810–960 cm^{-1} range), B—O—H bending modes (960–1180 cm^{-1}) and O—B—O bending modes (450–490 cm^{-1}). For the boric acid molecule, the mass-sensitivity is restricted to the anti-symmetric B—O stretching modes (1400–1450 cm^{-1}) and the out-of-plane symmetric O—B—O bending (640–670 cm^{-1}). At 300 K, the fractionation factor between isolated species ($\alpha_{34} = 1.0387$; Table 2) is slightly higher than that obtained in the previous studies and falls in the upper range of the DFT values computed by Rustad et al. (2010) ($\alpha_{34} =$ 1.036–1.040).

Seven of the atomic-scale models of boron-bearing carbonates of Balan et al. (2016) have been investigated (Table 1). Comparison with available NMR data (Sen

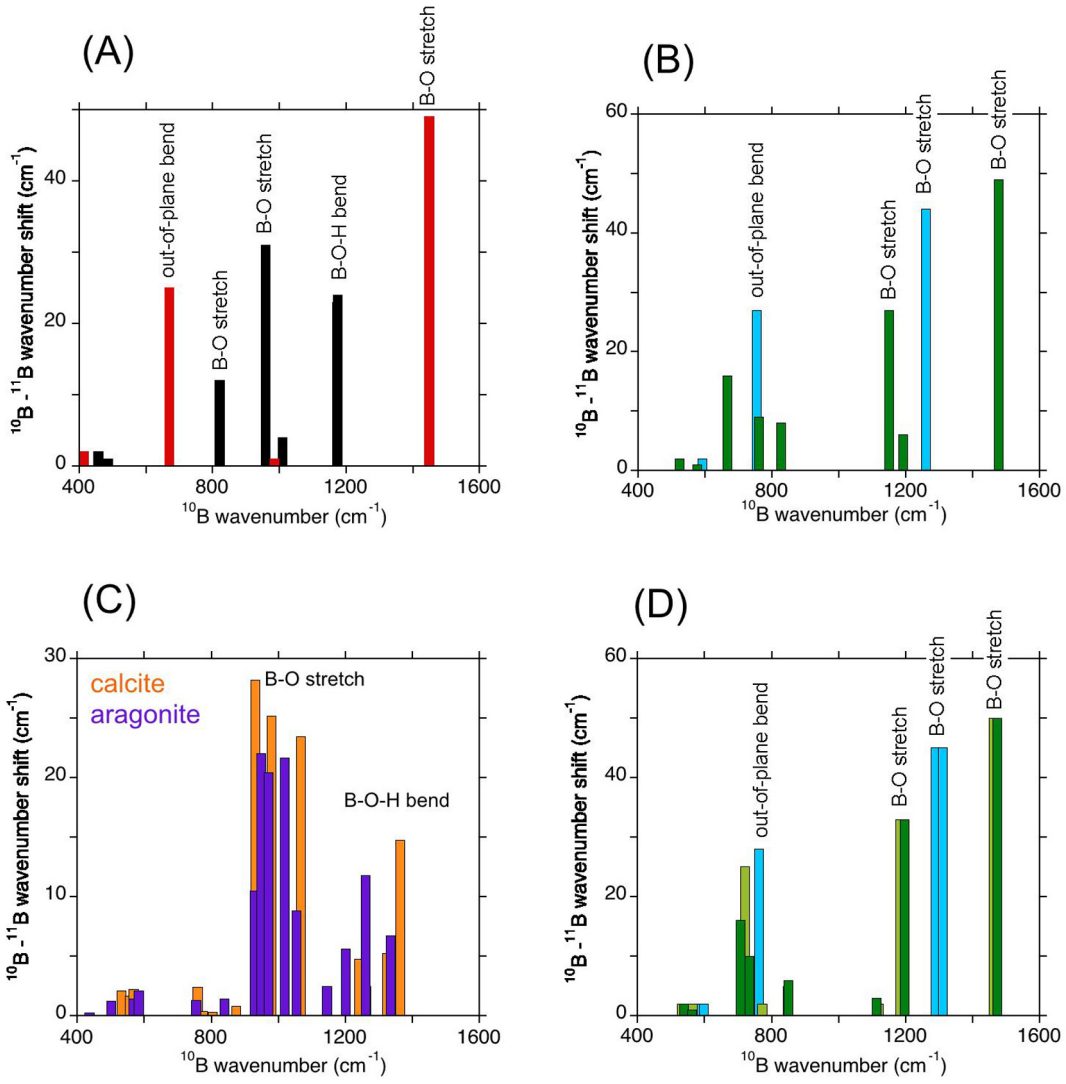

Fig. 1. Theoretical frequency variations induced by the ^{11}B for ^{10}B isotopic substitution of vibrational modes reported as a function of the frequencies computed for the ^{10}B systems. (A) Isolated species in vacuum: $B(OH)_4^-$ (black), $B(OH)_3$ (red); (B) Trigonal structural species in calcite: BO_3^{3-} (light blue), $BO_2(OH)^{2-}$ (green); (C) Tetragonal structural species $B(OH)_4^-$ in aragonite (purple) and calcite (orange); (D) Trigonal structural species in aragonite: BO_3^{3-} (light blue), $BO_2(OH)^{2-}$ (model A: green, model B: light green). (For interpretation of the references to colour in this figure legend, the reader is referred to the web version of this article.)

Table 2
Theoretical reduced partition function ratio (1000 ln(β)) and equilibrium fractionation factor between boric acid and borate ion (α_{34}) at 300 K for isolated species using different GGA functionals (PBE, BLYP) and basis sets (plane-waves, localized functions).

	PBE PW (This work)	PBE (6-311++G(2d,2p)) (Rustad et al., 2010)	BLYP PW (Kowalski et al., 2013)	BLYP (6-311 + G(d,p)) (Zeebe, 2005)
$B(OH)_3$	198.5	200.3	191.7	194.7
$B(OH)_4^-$	160.5	164.1	154.7	157.4
α_{34}	1.0387	1.0369	1.0377	1.0380

et al., 1994; Klochko et al., 2009; Rollion-Bard et al., 2011; Mavromatis et al., 2015) has shown that these models correspond to the most plausible environment of boron in calcite and aragonite. For trigonal boron, the two BO_3^{3-} models and the three lattice-neutral $BO_2(OH)^{2-}$ models have been considered. In aragonite, the two $BO_2(OH)^{2-}$ models (Table 1) correspond to the protonation of one of the two symmetrically non-equivalent oxygen belonging to the trigonal boron group (Balan et al., 2016). As for the isolated borate ion, the electrostatic compensation of the two $B(OH)_4^-$ and two BO_3^{3-} models (Table 1) is ensured by a counter-charge homogeneously spread over the system. The partially protonated tetrahedral $BO(OH)_3^{2-}$ species modeled in Balan et al. (2016) were not considered in the present study because their distortion is not consistent with experimental NMR observations (Sen et al., 1994).

The interaction of structural borate ions with the crystal host leads to structural distortions (Table 1) and produce a more complex vibrational pattern than that of isolated $B(OH)_4^-$ ions (Fig. 1, Table S2). Vibrational modes contributing to the isotopic fractionation display higher frequencies, leading to a higher RPFR for calcite and aragonite. The structural $B(OH)_4^-$ ions display slightly different equilibrium isotopic fractionation properties in these two structures. A ^{11}B enrichment of 2.6‰ in calcite with respect to aragonite is observed (Fig. 2). These observations are consistent with the fact that the similar average B—O lengths observed in the two crystal structures (1.48 Å) are shorter than the B—O length of the isolated borate (1.495 Å, Table 1).

In the BO_3^{3-} species, the isotopic fractionation is mostly related to the ν_3 (anti-symmetric B—O stretching in the range 1215–1311 cm^{-1}) and ν_2 (out-of-plane motion of B atom in the range 726–753 cm^{-1}) modes (Fig. 1, Table S3). In the less symmetric $BO_2(OH)^{2-}$ environment, the ν_3 modes are split and make the strongest contribution

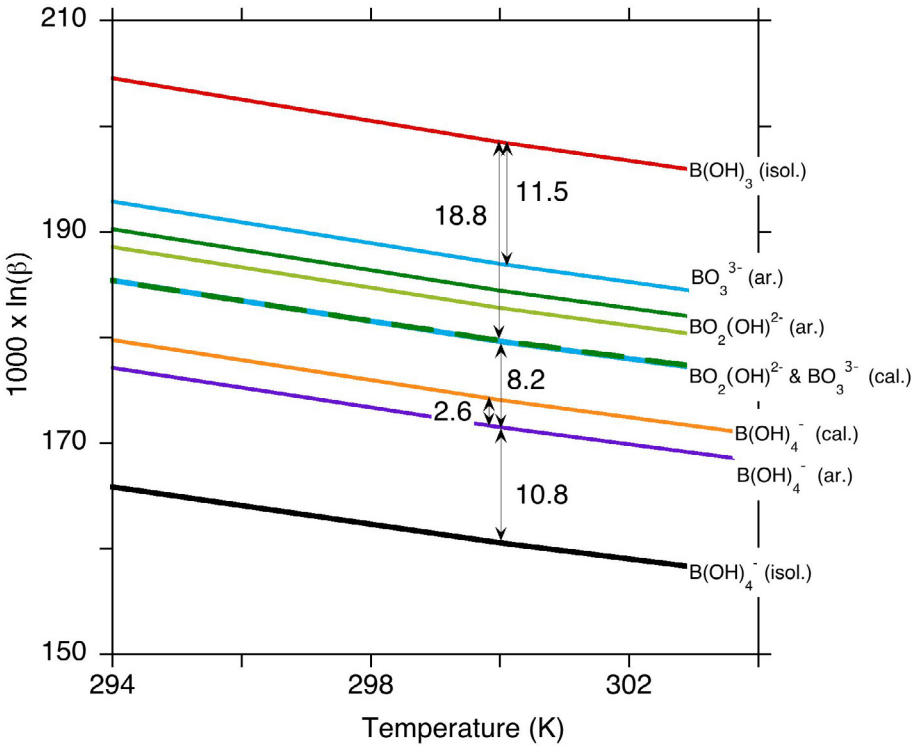

Fig. 2. Theoretical reduced partition function ratios as a function of temperature. Same colors as in Fig. 1. Selected fractionation coefficients between boron species at 300K are indicated in ‰ units. (For interpretation of the references to colour in this figure legend, the reader is referred to the web version of this article.)

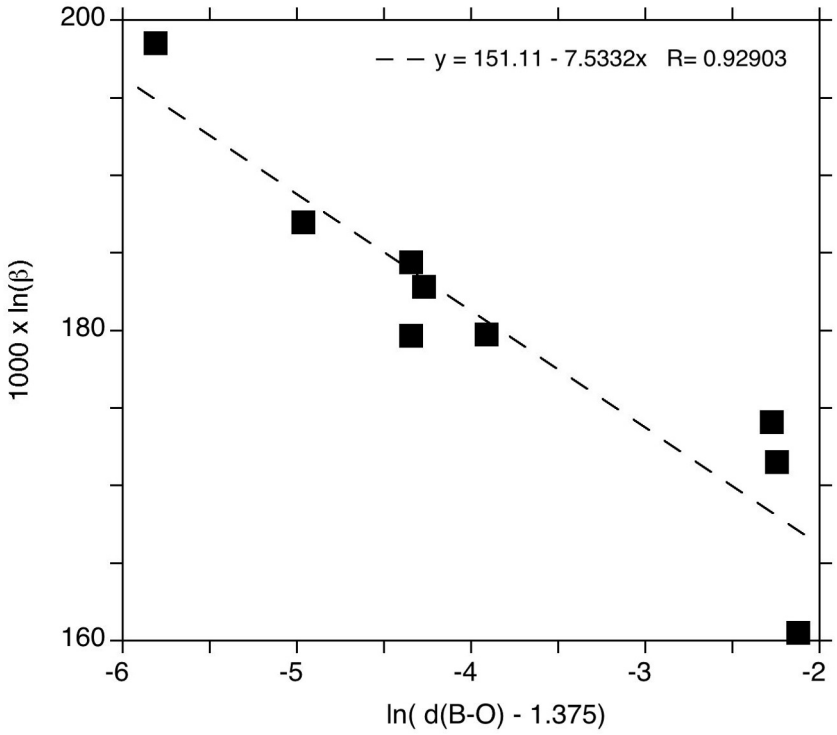

Fig. 3. Logarithmic plot of the theoretical reduced partition function ratios as a function of average B—O bond distance d(B—O) in Å.

to the fractionation, whereas additional contributions involving O—B—O bending modes are observed. Compared with the tetragonal species, a greater variability is observed among RPFRs of the trigonal $BO_2(OH)^{2-}$ and BO_3^{3-} species (Fig. 2). As expected from their shorter average B—O length (Table 1), trigonal species display higher RPFRs than tetrahedral ones, indicating a preferential enrichment in ^{11}B. Among the seven structural models, the highest RPFR is observed for BO_3^{3-} groups in aragonite which display the shortest average B—O bond length (1.382 Å). Their RPFR is however still lower than that computed for the isolated boric acid molecule, which displays even shorter B—O

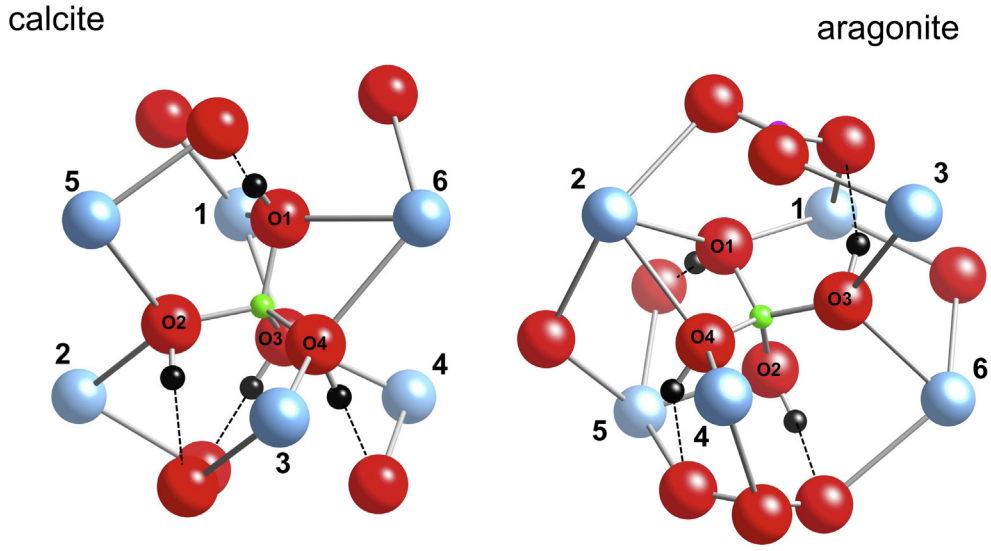

Fig. 4. Structural models of $B(OH)_4^-$ in calcium carbonates. The Ca atoms potentially substituted by Na atoms to ensure a local charge compensation are numbered from 1 to 6 for each model. The dotted lines indicate the H-bonding of OH groups with nearby oxygen atoms. Green: boron, red: oxygen, black: hydrogen, blue: calcium. (For interpretation of the references to colour in this figure legend, the reader is referred to the web version of this article.)

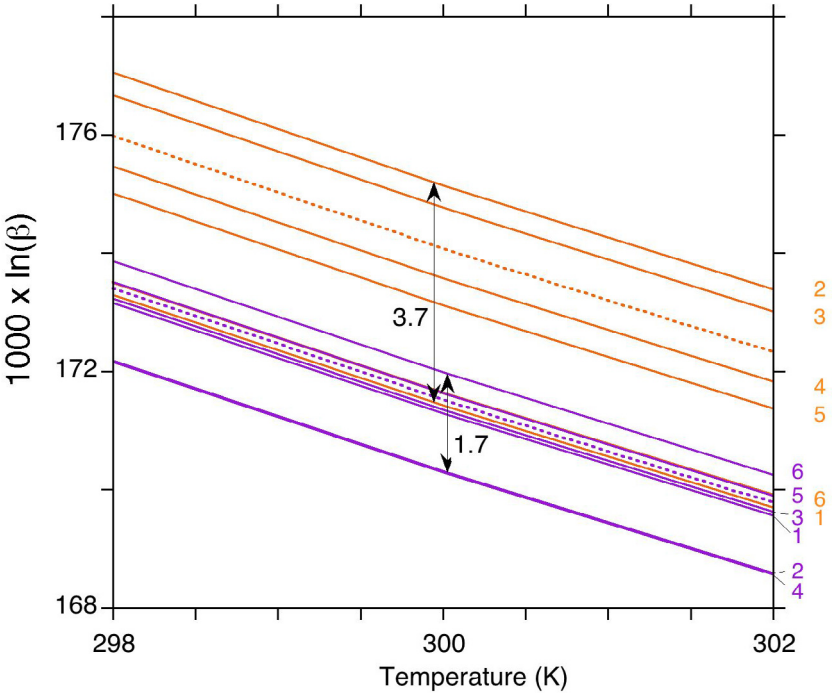

Fig. 5. Comparison of the theoretical reduced partition function ratios of structural $B(OH)_4^-$ computed with various charge compensation strategies: homogeneous electrostatic background (dotted lines) or local Na^+ for Ca^{2+} substitution (plain lines). The corresponding substitution sites (Fig. 4) are indicated on the right, and the same colours as in Figs. 1 and 2 are used here. (For interpretation of the references to colour in this figure legend, the reader is referred to the web version of this article.)

bonds (1.378 Å, Table 1). Overall, a correlation is observed on logarithmic plots between the RPFRs and average B—O bond length, the shorter bond lengths leading to higher RPFRs (Fig. 3). Similar correlations have been reported at high temperature for boron species by Kowalski et al. (2013) and for Si isotopes by Méheut and Schauble (2014).

The structural boron species thus display significant equilibrium isotopic fractionation with respect to isolated $B(OH)_3$ and $B(OH)_4^-$ in vacuum. At 300 K, structural borates are enriched in ^{11}B by 10.8–13.4‰ with respect to the isolated borate ions; whereas structural trigonal species are lighter than isolated boric acid molecules by 11.5–18.8‰. In the case of fully protonated borate ions, the specific mechanism of charge compensation (coupled substitution vs. homogeneous electrostatic background) only has a moderate effect on the defect geometry (Balan et al., 2016). To further document the sensitivity of structural borate ions to their local environment, the RPFR of models in which the charge compensation of the $B(OH)_4^-$ for CO_3^{2-} substitution is locally ensured by a Na^+ for Ca^{2+} substitution have been computed (Fig. 4). Although close to the results obtained on the two models compensated by a homogeneous electrostatic counter-charge, a variability of the RPFRs reaching 1.7‰ in aragonite and 3.7‰ in calcite is observed depending on the specific location of the Na ion in the crystal structure (Fig. 5). It is noteworthy that the properties of the homogeneously compensated models plot within the range covered by locally compensated models, sustaining the use of a homogeneous electrostatic background to investigate the properties of structural defects displaying an electrostatic charge imbalance.

4. DISCUSSION

4.1. Uncertainties in the theoretical prediction of isotopic fractionation properties of solid phases and isolated molecules

As discussed by, e.g., Schauble et al. (2006), Méheut et al. (2007) or Dupuis et al. (2015), the various approximations used in the modeling strategy may affect the theoretical isotopic fractionation properties. Most of these approximations, such as those related to the specific exchange-correlation functional and type of basis sets chosen to compute the total energy and electronic structure of the systems, lead to systematic errors that mostly cancel when comparing RPFR obtained at the same theoretical level. The neglect of chemical bond anharmonicity is also usually considered as a source of systematic error (Méheut et al., 2007) but in the present case it could differently affect the RPFR values of trigonal and tetrahedral boron species. As a full anharmonic treatment of large systems at a first-principles theoretical level is not feasible using current computational capacities, the potential contribution of anharmonicity to observed fractionation factors is difficult to assess. Useful information can be obtained by comparing available experimental data to the theoretical harmonic frequencies of reference systems displaying trigonal or tetrahedral boron species: isolated boric

acid molecule ($B(OH)_3$) and two solid phases, takedaite ($Ca_3B_2O_6$) and teepleite ($Na_2B(OH)_4Cl$). This comparison (Fig. S2) indicates that the theoretical frequencies underestimate the experimental ones by ~2%, which is well consistent with other modeling studies using the PBE functional (e.g. Schauble et al., 2006) and should translate to a similar variation of the fractionation factors expressed in ‰ (Méheut et al., 2009). The comparison does not reveal any significant difference in the quality of the harmonic treatment for the various reference systems, which indicates that anharmonicity can actually be considered as a systematic effect in the present study. This should be particularly true when the properties of the same species occurring in different phases, e.g. $B(OH)_4^-$ in vacuum or in crystalline structures, are compared. For this reason, it is reasonable to consider that the relative uncertainty related to the theoretical fractionation factors observed between solid phases and molecules in vacuum does not exceed a few percents. Actually, the major source of uncertainty of the present approach lies in the models of the boron bearing carbonates. Although the search for minimal energy configurations and the comparison with available NMR data sustain their relevance as the most probable geometric configurations of structural boron species (Balan et al., 2016), vibrational spectroscopic data, such as those recently obtained for structural sulfate in calcite (Balan et al., 2017), would be an important but still lacking information on the local environment of borate in calcium carbonates.

4.2. Effect of solvation on the reduced partition function ratio of aqueous boron species

A major difficulty in the theoretical study of isotopic equilibrium between solids and solution is related to the determination of the RPFR of aqueous species. Interaction of the solute species with water molecules as well as the electrostatic polarization of the solvent are expected to modify their structural, vibrational and isotopic fractionation properties with respect to those determined in vacuum. These effects can be taken into account by polarizable continuum models or by explicitly modeling the solvation shells, either using finite-size clusters or periodic models. An explicit treatment of solvation by water molecules is recommended to model the properties of aqueous molecular species (Liu and Tossell, 2005; Rustad et al., 2008) for which hydrogen bond sharing with the solvent molecules is expected to play an important role.

In a theoretical modeling study of boron isotopic fractionation in aqueous solutions, Rustad et al. (2010) determined the RPFR of aqueous borate and boric acid on large 32-water clusters generated from *ab initio* molecular dynamic runs. The harmonic vibrational properties of the clusters were computed using various theoretical approaches, including DFT calculations. In the case of aqueous boron, and at variance with other systems such as Li isotopes, the use of the harmonic approximation is validated by the persistence of the B coordination state

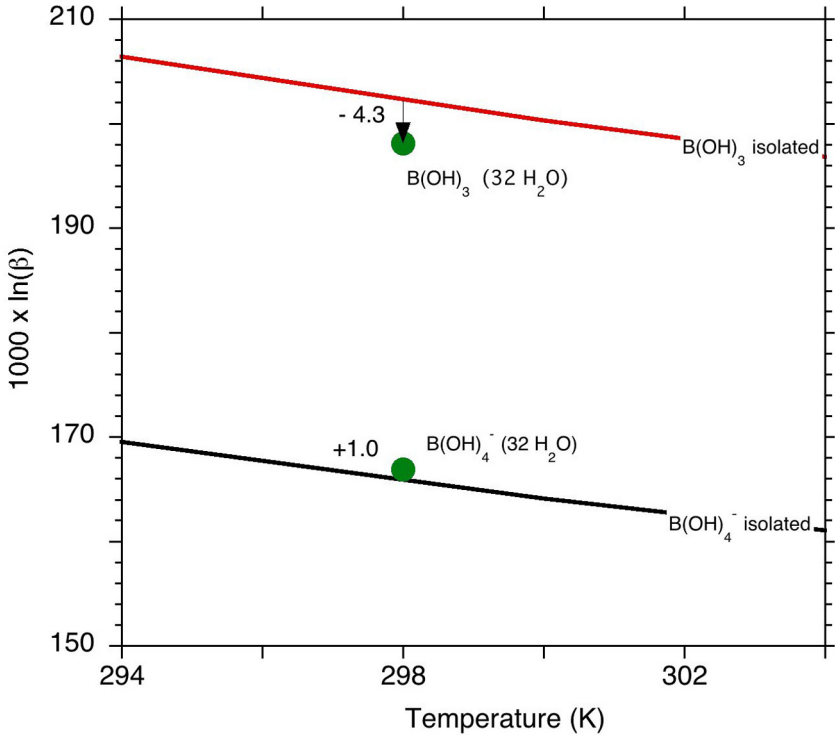

Fig. 6. Comparison of the theoretical reduced partition function ratios of isolated $B(OH)_4^-$ (black line) and $B(OH)_3$ (red line) species with corresponding aqueous values (green circles) based on data from Rustad et al. (2010). For aqueous boric acid, the used value does not include contributions from tetrahedral Lewis complexes ($B(OH)_3 \cdot H_2O$). (For interpretation of the references to colour in this figure legend, the reader is referred to the web version of this article.)

during the simulations (Dupuis et al., 2017). It is thus possible to assess solvation effects on the isotopic fractionation properties of boron species by comparing the RPFR values of aqueous clusters to those of isolated species computed at the same theoretical level (1.2244 and 1.1805 at 298 K for isolated boric acid and borate, respectively, using the 6-311++G(2d,2p) basis set). Assuming a +0.0017 shift of the large aqueous clusters RPFR related to the use of the slightly reduced 6-311++G** basis set (Rustad et al., 2010), the comparison indicates that hydration of boric acid molecules decreases their RPFR by ~4.3‰ at 298 K (Fig. 6). This value does not consider the contributions of two tetrahedral Lewis complexes ($B(OH)_3 \cdot H_2O$) computed by Rustad et al. (2010). It is close to that inferred by Liu and Tossell (2005) from the analysis of cluster models containing up to 34 water molecules, i.e. ~3.5‰ at the same temperature. A decrease in the RPFR of boric acid between the isolated and aqueous species is also consistent with the lowering of the anti-symmetric B—O stretching frequency experimentally observed between gas-phase and solution (1429 cm^{-1} in vapour, Gilson, 1991; 1410 cm^{-1} in aqueous solution, Peak et al., 2003). A weaker but reverse effect of solvation is expected for the borate ions, the hydration increasing their RPFR by ~1.0‰ (Fig. 6). This increase can be ascribed to a frequency blue-shift of B—O—H bending and anti-symmetric B—O stretching modes, as previously noted by Rustad and Bylaska (2007). A blue shift of the symmetric B—O stretching mode in hydrated borate clusters was also reported by Zhou et al. (2013). Incidentally, this suggests that the mode experimentally observed in aqueous solution at 975 cm^{-1} (e.g. Sanchez-Valle et al., 2005) is actually related to the anti-symmetric stretching of B—O bonds.

The hydration of boron species thus tends to reduce the theoretical fractionation factor between aqueous $B(OH)_3$ and $B(OH)_4^-$ by 4–5‰ with respect to that calculated between isolated species in vacuum. Based on the present analysis, the borate ions in the structure of calcium carbonates appear as heavier than their aqueous counterparts by ~10 to 13‰ at 300 K. The theoretical fractionation factor between aqueous boric acid and the two trigonal boron species in calcite is ~−14.5‰. For aragonite, the theoretical fractionation between boric acid and trigonal species is smaller (average value of ~−10.5‰ for the two $BO_2(OH)^{2-}$ and ~−7‰ for the BO_3^{3-} species).

Compared with isotopic fractionation involving small molecules or crystalline solids, the determination of isotopic fractionation properties in aqueous solution is also affected by the slowly converging character of thermodynamic quantities as a function of the system size and simulation length (e.g. Blanchard et al., 2017). The uncertainty related to the limited sampling of the configuration space could therefore be more significant when considering aqueous species (Kowalski et al., 2013) but should be minimized by an appropriate statistical sampling. The standard errors on the RPFR of aqueous borate and boric acid resulting from the average of 8 configurations by Rustad et al. (2010) is typically smaller than 0.5‰. It is noteworthy that Liu and Tossell (2005) suggest that solvation could instead decrease the RPFR of the borate ions with respect to the isolated one by 3.7‰ at 300 K. In this case, the B isotopic fractionation of borate between the aqueous solution and the heavier solid phase should increase with respect to that involving isolated borate in vacuum (Fig. 2). Thus, although some uncertainty may affect the quantitative prediction of the solvation effect, this uncertainty should not exceed a few per mil and should not modify the qualitative picture inferred from the theoretical fractionation factors calculated between solids and isolated species in vacuum.

4.3. Implications for the incorporation mechanism of boron in carbonates

As discussed in the preceding parts, the numerous approximations involved in the calculation of isotopic fractionation factors between solids and solutions prevent a straightforward comparison of the theoretical values with experimental data. As a matter of fact, the RPFR values reported by Rustad et al. (2010) using the PBE functional lead to a theoretical fractionation factor between the two aqueous boron species $\alpha_{34} = 1.0318$. Although this value is in reasonable agreement with the experimental value of $\alpha_{34} = 1.0308$ determined in pure water at 25 °C by Klochko et al. (2006), it is larger than that reported in synthetic seawater or 0.6 N KCl solution ($\alpha_{34} = 1.0272/1.025$). More recently, Nir et al. (2015) also reported a fractionation of 26 ± 1‰ for various salinities (0.05 M NaCl; seawater). Even though calculations on aqueous boron clusters containing alkaline and alkaline-earth cations (Liu and Tossell, 2005) suggest that their presence could affect the

Table 3
Experimental parameters of the synthetic samples investigated by Mavromatis et al. (2015) and Noireaux et al. (2015). B4: tetrahedral boron.

	Sample	pH	% B4 solid	$\delta^{11}B$ solid	%B4 solution	$\delta^{11}B$ B4 solut.
Calcite	8	7.52	35 (±20)	−16.6	2.7	−25.4
	111	7.99	85 (±10)	−16.7	7.3	−24.3
	12	8.34	40 (±10)	−14.9	15.0	−22.3
	46	8.64	40 (±15)	−13.1	28.2	−19.0
	85	8.88	77 (±20)	−11.0	40.6	−15.8
Aragonite	9	7.58	85 (±5)	−24.6	4	−25.1
	87	8.88	87 (±5)	−14.7	45.4	−14.6

RPFR of aqueous boron species, the theoretical assessment of salinity effects on isotopic fractionation properties is a challenging task. Considering that uncertainties also affect the experimental determination of fractionation factors in solution, a perfect agreement between theory and experiment would most likely be fortuitous. Nonetheless, the theoretical analysis reveals important features of the equilibrium isotopic fractionation properties of boron in carbonates at ambient temperature that can be used to discuss available experimental data. First, the fractionation factors involving structural tetrahedral borates should not differ by more than 3‰ in aragonite and in calcite. Second, a fractionation larger than 5‰ is expected between structural trigonal and tetrahedral species. Third, a ^{11}B enrichment of the structural borates reaching 10‰ can be expected at equilibrium with respect to the aqueous borate.

Recently, Mavromatis et al. (2015) and Noireaux et al. (2015) conducted experimental studies combining isotopic composition measurements and determination of the solid-state boron speciation on synthetic calcite and aragonite samples grown under low-supersaturation conditions (Table 3). For the aragonite samples, their composition nearly matches that calculated for the aqueous borate ion based on Nir et al. (2015) α_{34} experimental value. The observed isotopic fractionation thus appears as almost nil. In particular, it is significantly smaller than the one expected from the present theoretical modeling (~10‰). At this point, several interpretations can be proposed. On the one hand, it could be assumed that isotopic equilibrium has been reached during the slow growth of crystals, which would imply that the theoretical fractionation values are severely overestimated. Considering that the properties of the structural and isolated borate in vacuum have been determined at the same theoretical level and that in both cases similar anharmonic contributions are expected, it turns out that the actual solvation effect on the RPFR of aqueous borate would be much larger than the one inferred in the preceding part (~+1‰). Although it is not possible to fully rule out this possibility, the specific reasons for such a theoretical underestimation of the solvation effect are not apparent. On the other hand, the lack of isotopic fractionation between the solid and the solution could indicate an out-of-equilibrium incorporation of boron without noticeable fractionation, e.g. involving a local equilibrium of the solution with an adsorbed borate species displaying a RPFR smaller than that of the structural species modeled here.

In contrast, the calcite samples display a significant enrichment in ^{11}B with respect to aqueous borate that cannot be modeled over the whole range of pH (7.5–9) using a single isotopic fractionation factor (Fig. 7). The fractionation factor would be above 8‰ at lower pH but would decrease to below 5‰ at high pH. It is worth to note that the isotopic composition of the calcite samples smoothly follows the pH variation, whereas the proportion of trigonal boron displays variations from ~15 to ~65% of total boron from one sample to another (Table 3). Assuming that boric acid and borate are incorporated into the crystal structure with no isotope fractionation, Noireaux et al. (2015) interpreted the experimental observations as related

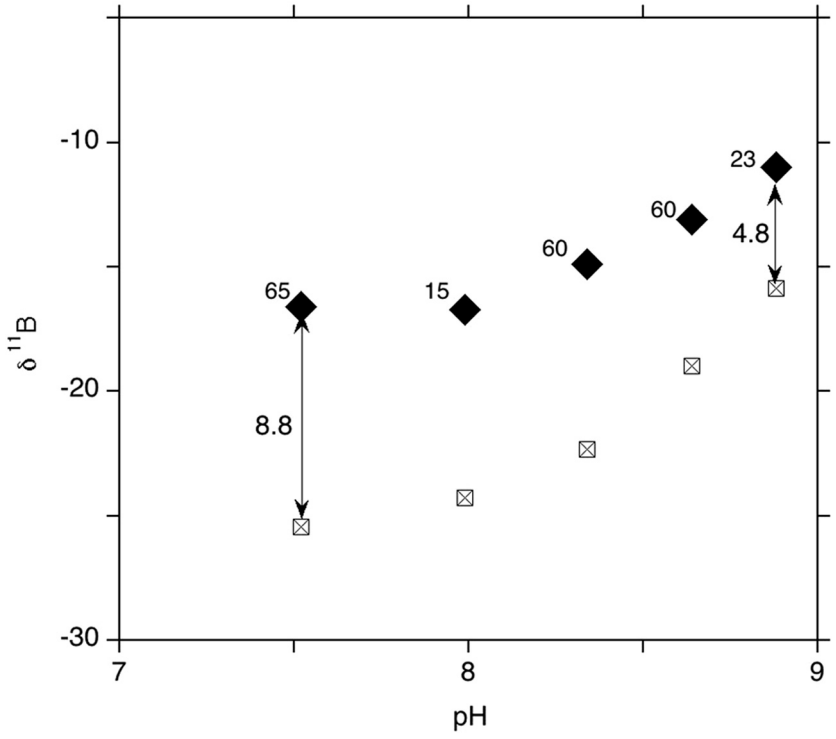

Fig. 7. Isotopic composition of the calcite samples precipitated by Noireaux et al. (2015) (black diamonds) and aqueous borate composition (open squares) determined using $\alpha_{34} = 1.026$ and PHREEQC calculations (Parkhurst and Appelo, 2013). The NMR-determined fraction of trigonal boron is indicated as % value near the experimental points.

to the incorporation of various proportions of the trigonal and tetragonal aqueous species in the solid phase. However, the proportions matching the isotopic compositions differ from those inferred from NMR measurements.

The sign and the range of magnitude of the fractionation observed between calcite and aqueous borate at low pH (Fig. 7) are roughly consistent with the equilibrium fractionation theoretically inferred between aqueous and tetrahedral borate in calcite. The apparent independence of the experimental fractionation on the solid-state speciation of boron and growth rate (Noireaux et al., 2015) also points to close-to-equilibrium conditions. The relatively fast coordination change of boron species in aqueous solution compared with the slow carbonate growth rates should limit potential kinetic isotopic fractionation (Zeebe et al., 2001). However, the lack of correlation between the NMR-determined fraction of trigonal and tetrahedral boron and the observed isotopic composition of calcite (Fig. 7) questions a model in which both the trigonal and tetrahedral boron species would be in isotopic equilibrium with the solution considering that a fractionation factor of ~5.6‰ is theoretically expected between the two species (Fig. 2). Thus, the present theoretical results could sustain a model in which the isotopic composition of calcite is acquired through equilibrium of adsorbed borate ions with the aqueous solution, followed by a partial coordination change of tetrahedral to trigonal species in which boron does not isotopically re-equilibrate with the solution, as initially proposed by Hemming and Hanson (1992). We note that Kaczmarek et al. (2016) reported a significantly smaller isotopic fractionation between aqueous and incorporated borate ions in calcite samples synthesized at higher ionic strength, 0.75 M vs. 0.1 M NaCl for Noireaux et al. (2015). The different synthesis conditions could favor an out-of-equilibrium entrapment of boron in the solid phase similar to that observed in aragonite.

5. CONCLUSION

In the present work, the theoretical equilibrium isotopic fractionation properties of major structural boron species in calcite and aragonite have been determined. For both crystalline hosts, the tetrahedral species display RPFRs significantly higher than that determined for isolated borate ion in vacuum. Although borate hydration increases its RPFR by ~1‰, structural borates are still enriched by more than 10‰ with respect to their aqueous counterparts at ambient temperature, indicating that isotopic fractionation during borate incorporation in carbonates cannot be a priori neglected. Compared with structural borate, higher RPFRs are computed for trigonal species, with the highest values in aragonite. The present results also confirm that the boron isotopic composition in solids can be affected by variations in the medium-range environment of the B impurity, i.e. farther than the first coordination shell, and should not be interpreted solely in the light of trigonal to tetragonal boron ratio. They further document the importance to take into account the site-specific properties of trace molecular species in minerals to interpret their isotopic composition (Rustad and Zarzycki, 2008).

Based on these theoretical results, the experimentally determined isotopic composition and NMR speciation of boron in synthetic calcium carbonate samples (Noireaux et al., 2015) suggests that neither boron incorporated in aragonite nor in calcite is in isotopic equilibrium with boron in the aqueous solution. This further suggests that borate adsorption is a key step in the record of aqueous boron isotopic composition by calcium carbonates, as previously proposed by, e.g., Hemming et al. (1998) or Ruiz-Agudo et al. (2012). The structural incorporation of boric acid molecule in crystalline carbonates is unlikely but could occur in more disordered calcium carbonate phases, such as those observed at the crystallization center of aragonitic corals (Rollion-Bard et al., 2011). Beside classical growth mechanisms involving the ion by ion attachment to mineral advancing steps, other pathways may indeed prevail during the formation of carbonates under elevated supersaturation conditions, involving the transient formation of amorphous calcium carbonate (ACC) phases (Gower, 2008; Mavromatis et al., 2017). Although a modeling of such mechanism is out of the scope of the present study, it can be noticed that the Mg isotopic signature of calcite formed via ACC precursors does not reflect that of the precursors, as the transformations occur through dissolution-precipitation mechanisms (Mavromatis et al., 2017). The present theoretical results point to the need of further experimental and theoretical investigations, especially of the mechanisms of boron adsorption at the surface of calcium carbonates – the first step in B incorporation in the crystal structure – and the kinetics of structural and isotopic equilibration of boron co-precipitated with $CaCO_3$ polymorphs.

ACKNOWLEDGMENTS

We thank Prof. Yun Liu and two anonymous reviewers for their constructive comments. This work has been supported by the French National Research Agency through the CARBORIC (ANR-13-BS06-0013-06) project. This work was performed using HPC resources from GENCI-IDRIS (Grant 2017-A0010401519). This is a LabEx MATISSE contribution.

APPENDIX A. SUPPLEMENTARY DATA

Supplementary data associated with this article can be found, in the online version, at https://doi.org/10.1016/j.gca.2017.10.017.

REFERENCES

Balan E., Blanchard M., Pinilla C. and Lazzeri M. (2014) First-principles modeling of sulfate incorporation and $^{34}S/^{32}S$ isotopic fractionation in different calcium carbonates. *Chem. Geol.* **374–375**, 84–91.

Balan E., Pietrucci F., Gervais C., Blanchard M., Schott J. and Gaillardet J. (2016) First-principles study of boron speciation in calcite and aragonite. *Geochim. Cosmochim. Acta* **193**, 119–131.

Balan E., Aufort J., Pouillé S., Dabos M., Blanchard M., Lazzeri M., Rollion-Bard C. and Blamart D. (2017) Infrared spectroscopic study of sulfate-bearing calcite from deep-sea bamboo coral. *Eur. J. Mineral.* **29**, 397–408.

Baroni S., de Gironcoli S., Dal Corso A. and Giannozzi P. (2001) Phonons and related crystal properties from density-functional perturbation theory. *Rev. Mod. Phys.* **73**, 515–561.

Bigeleisen J. and Mayer M. G. (1947) Calculation of equilibrium constants for isotopic exchange reactions. *J. Chem. Phys.* **15**, 261–267.

Blanchard M., Balan E. and Schauble E. (2017) Equilibrium fractionation of non-traditional isotopes: a molecular modeling perspective. *Rev. Mineral. Geochem.* **82**, 27–63.

Branson O., Kaczmarek K., Refern S. A. T., Misra S., Langer G., Tyliszczak T., Bijma J. and Elderfield H. (2015) The coordination and distribution of B in foraminiferal calcite. *Earth Planet. Sci. Lett.* **416**, 67–72.

DePaolo D. J. (2011) Surface kinetic model for isotopic and trace element fractionation during precipitation of calcite from aqueous solutions. *Geochim. Cosmochim. Acta* **75**, 1039–1056.

Dupuis R., Benoit M., Nardin E. and Méheut M. (2015) Fractionation of silicon isotopes in liquids: the importance of configurational disorder. *Chem. Geol.* **396**, 239–254.

Dupuis R., Benoit M., Tuckerman M. E. and Méheut M. (2017) Importance of a Fully Anharmonic treatment of equilibrium isotope fractionation properties of dissolved ionic species as evidenced by Li^{+}(aq). *Acc. Chem. Res.* **50**, 1597–1605.

Gabitov R. I., Rollion-Bard C., Tripati A. and Sadekov A. (2014) In situ study of boron partitioning between calcite and fluid at different crystal growth rates. *Geochim. Cosmochim. Acta* **137**, 81–92.

Garrity K. F., Bennett J. W., Rabe K. M. and Vanderbilt D. (2014) Pseudopotentials for high-throuhput DFT calculations. *Comput. Mater. Sci.* **81**, 446–452.

Giannozzi P., Baroni S., Bonini N., Calandra M., Car R., Cavazzoni C., Ceresoli D., Chiarotti G.L., Cococcioni M., Dabo I., Dal Corso A., de Gironcoli S., Fabris S., Fratesi G., Gebauer R., Gerstmann U., Gougoussis C., Kokalj A., Lazzeri M., Martin-Samos L., Marzari N., Mauri F., Mazzarello R., Paolini S., Pasquarello A., Paulatto L., Sbraccia C., Scandolo S., Sclauzero G., Seitsonen A.P., Smogunov A., Umari P. and Wentzcovitch R.M. (2009) Quantum ESPRESSO: a modular and open-source software project for quantum simulations of materials. *J. Phys.: Cond. Matt.* **21**, 395502.

Gilson T. R. (1991) Characterisation of ortho- and meta-boric acids in the vapour phase. *J. Chem. Soc. Dalton Trans.*, 2463–2466.

Gower L. B. (2008) Biomimetic model systems for investigating the amorphous precursor pathway and its role in biomineralization. *Chem. Rev.* **108**, 4551–4627.

Hemming N. G. and Hanson G. N. (1992) Boron isotopic composition and concentration in modern marine carbonates. *Geochim. Cosmochim. Acta* **56**, 537–543.

Hemming N. G., Reeder R. J. and Hart S. R. (1998) Growth-step-selective incorporation of boron on the calcite surface. *Geochim. Cosmochim. Acta* **62**, 2915–2922.

Hobbs M. Y. and Reardon E. J. (1999) Effect of pH on boron coprecipitation by calcite: further evidence for nonequilibrium partitioning of trace elements. *Geochim. Cosmochim. Acta* **63**, 1013–1021.

Kaczmarek K., Nehrke G., Misra S., Bijma J. and Elderfield H. (2016) Investigating the effects of growth rate and temperature on the B/Ca ratio and $\delta^{11}B$ during inorganic calcite formation. *Chem. Geol.* **421**, 81–92.

Klochko K., Kaufman A. J., Yao W., Byrne R. H. and Tossell J. A. (2006) Experimental measurement of boron isotope fractionation in seawater. *Earth Planet. Sci. Lett.* **248**, 276–285.

Klochko K., Cody G. D., Tossell J. A., Dera P. and Kaufman A. J. (2009) Re-evaluating boron speciation in biogenic calcite and aragonite ^{11}B MAS NMR. *Geochim. Cosmochim. Acta* **73**, 1890–1900.

Kowalski P. M., Wunder B. and Jahn S. (2013) Ab initio prediction of equilibrium boron isotope fractionation between minerals and aqueous fluids at high P and T. *Geochim. Cosmochim. Acta* **101**, 285–301.

Lemarchand E., Schott J. and Gaillardet J. (2005) Boron isotopic fractionation related to boron sorption on humic acid and the structure of surface complexes formed. *Geochim. Cosmochim. Acta* **69**, 3519–3533.

Lemarchand E., Schott J. and Gaillardet J. (2007) How surface complexes impact boron isotope fractionation: evidence from Fe and Mn oxides sorption experiments. *Earth Planet. Sci. Lett.* **260**, 277–296.

Liu Y. and Tossell J. A. (2005) Ab initio molecular orbital calculations for boron isotope fractionations on boric acids and borates. *Geochim. Cosmochim. Acta* **69**, 3995–4006.

Liu Q., Tossell J. A. and Liu Y. (2010) On the proper use of the Bigeleisen–Mayer equation and corrections to it in the calculation of isotopic fractionation equilibrium constants. *Geochim. Cosmochim. Acta* **74**, 6965–6983.

Mavromatis V., Gautier Q., Bosc O. and Schott J. (2013) Kinetics of Mg partition and stable isotope fractionation during its incorporation in calcite. *Geochim. Cosmochim. Acta* **114**, 188–203.

Mavromatis V., Montouillout V., Noireaux J., Gaillardet J. and Schott J. (2015) Characterization of boron incorporation and speciation in calcite and aragonite from co-precipitation experiments under controlled pH, temperature and precipitation rate *Geochim. Cosmochim. Acta* **150**, 299–313.

Mavromatis V., Purgstaller B., Dietzel M., Buhl D., Immenhauser A. and Schott J. (2017) Impact of amorphous precursor phases on magnesium isotope signatures of Mg-calcite. *Earth Planet. Sci. Lett.* **464**, 227–236.

Méheut M., Lazzeri M., Balan E. and Mauri F. (2007) Equilibrium isotopic fractionation in the kaolinite, quartz, water system: prediction from first principles density-functional theory. *Geochim. Cosmochim. Acta* **71**, 3170–3181.

Méheut M., Lazzeri M., Balan E. and Mauri F. (2009) Structural control over equilibrium silicon and oxygen isotopic fractionation: a first-principles density-functional theory study. *Chem. Geol.* **258**, 28–37.

Méheut M. and Schauble E. A. (2014) Silicon isotope fractionation in silicate minerals: insights from first-principles models of phyllosilicates, albite and pyrope. *Geochim. Cosmochim. Acta* **134**, 137–154.

Nir O., Vengosh A., Harkness J. S., Dwyer G. S. and Lahav O. (2015) Direct measurement of the boron isotope fractionation factor: reducing the uncertainty in reconstructing ocean paleo-pH. *Earth Planet. Sci. Lett.* **414**, 1–5.

Noireaux J., Mavromatis V., Gaillardet J., Schott J., Montouillout V., Louvat P., Rollion-Bard C. and Neuville D. R. (2015) Crystallographic control on the boron isotope paleo-pH proxy. *Earth Planet. Sci. Lett.* **430**, 398–407.

Parkhurst D. L. and Appelo C. (2013) Description of input and examples for PHREEQC version 3: a computer program for speciation, batch-reaction, one-dimensional transport, and inverse geochemical calculations. USGS Numbered Series 6–A43, U.S. Geological Survey, Reston, VA.

Peak D., Luther G. W. and Sparks D. L. (2003) ATR-FTIR spectroscopic studies of boric acid adsorption on hydrous ferric oxide. *Geochim. Cosmochim. Acta* **67**, 2551–2560.

Perdew J. P., Burke K. and Ernzerhof M. (1996) Generalized gradient approximation made simple. *Phys. Rev. Lett.* **77**, 3865–3868.

Richet P., Bottinga Y. and Javoy M. (1977) A review of hydrogen, carbon, nitrogen, oxygen, sulphur, and chlorine stable isotope fractionation among gaseous molecules. *Ann. Rev. Earth Planet. Sci.* **5**, 65–110.

Rollion-Bard C., Blamart D., Trebosc J., Tricot G., Mussi A. and Cuif J.-P. (2011) Boron isotops as a pH proxy: a new look at boron speciation in deep-sea corals using ^{11}B MAS NMR and EELS. *Geochim. Cosmochim. Acta* **75**, 1003–1012.

Ruiz-Agudo E., Putnis C. V., Kowacz M., Ortega-Huertas M. and Putnis A. (2012) Boron incorporation into calcite during growth: Implications for the use of boron in carbonates as a pH proxy. *Earth Planet. Sci. Lett.* **345–348**, 9–17.

Rustad J. R. and Bylaska E. J. (2007) *Ab initio* calculation of isotopic fractionation in $B(OH)_{3(aq)}$ and $B(OH)_{4(aq)}^-$. *J. Am. Chem. Soc.* **129**, 2222–2223.

Rustad J. R., Nelmes S. L., Jackson V. E. and Dixon D. A. (2008) Quantum-chemical calculations of carbon-isotope fractionation in CO_2(g), aqueous carbonate species, and carbonate minerals. *J. Phys. Chem. A* **112**, 542–555.

Rustad J. R. and Zarzycki P. (2008) Calculation of site-specific carbon-isotope fractionation in pedogenic oxide minerals. *Proc. Nat. Acad. Sci.* **105**, 0297–10301.

Rustad J. R., Bylaska E. J., Jackson V. E. and Dixon D. A. (2010) Calculation of boron-isotope fractionation between $B(OH)_{3(aq)}$ and $B(OH)_{4(aq)}^-$. *Geochim. Cosmochim. Acta* **74**, 2843–2850.

Rustad J.R. (2016) Computational isotope geochemistry. In: Molecular Modeling of Geochemical Reactions: An Introduction (ed. J. D. Kubicki). pp. 151–176.

Sanchez-Valle C., Reynard B., Daniel I., Lecuyer C., Martinez I. and Chervin J. C. (2005) Boron isotopic fractionation between minerals and fluids: new insights from in situ high pressure-high temperature vibrational spectroscopic data. *Geochim. Cosmochim. Acta* **69**, 4301–4313.

Schauble E. A., Ghosh P. and Eiler J. M. (2006) Preferential formation of ^{13}C–^{18}O bonds in carbonate minerals, estimated using first-principles lattice dynamics. *Geochim. Cosmochim. Acta* **70**, 2510–2529.

Sen S., Stebbins J. F., Hemming N. G. and Ghosh B. (1994) Coordination environments of B impurities in calcite and aragonite polymorphs: a ^{11}B MAS NMR study. *Am. Mineral.* **79**, 819–825.

Spivack A. J., You C. and Smith H. J. (1993) Foraminiferal boron isotope ratios as a proxy for surface ocean pH over the past 21 Myr. *Nature* **363**, 149–151.

Stewart J. A., Anagnostou E. and Foster G. L. (2016) An improved boron isotope pH proxy calibration for the deep-sea coral Desmophyllum dianthus through sub-sampling of fibrous aragonite. *Chem. Geol.* **447**, 148–160.

Tossell J. A. (2005) Boric acid, "carbonic" acid, and N-containing oxyacids in aqueous solution: *ab initio* studies of structure, pKa, NMR shifts, and isotopic fractionations. *Geochim. Cosmochim. Acta* **69**, 5647–5658.

Tossell J. A. (2006) Boric acid adsorption on humic acids: ab initio calculation of structures, stabilities, ^{11}B NMR and ^{11}B,^{10}B isotopic fractionations of surface complexes. *Geochim. Cosmochim. Acta* **70**, 5089–5103.

Uchikawa J., Penman D. E., Zachos J. C. and Zeebe R. E. (2015) Experimental evidence of kinetic effects on B/Ca in synthetic calcite: implications for potential $B(OH)_4^-$ and $B(OH)_3$ incorporation. *Geochim. Cosmochim. Acta* **150**, 171–191.

Vengosh A., Kolodny Y., Starinsky A., Chivas A. R. and McCulloch M. T. (1991) Coprecipitation and isotopic fractionation of boron in modern biogenic carbonates. *Geochim. Cosmochim. Acta* **55**, 2901–2910.

Watson E. B. (2004) A conceptual model for near-surface kinetic controls on the trace-element and stable isotope composition of abiogenic calcite crystals. *Geochim. Cosmochim. Acta* **68**, 1473–1488.

Watkins J. M., DePaolo D. J. and Watson E. B. (2017) Kinetic fractionation of non-traditional stable isotopes by diffusion and crystal growth reactions. *Rev. Mineral. Geochem.* **82**, 85–125.

Zeebe R. E., Sanyal A., Ortiz J. D. and Wolf-Gladrow D. A. (2001) A theoretical study of the kinetics of the boric acid – borate equilibrium in seawater. *Mar. Chem.* **74**, 113–124.

Zeebe R. E. (2005) Stable boron isotope fractionation between dissolved $B(OH)_3$ and $B(OH)_4^-$. *Geochim. Cosmochim. Acta* **69**, 2753–2766.

Zhang S., Henehan M. J., Hull P. M., Reid R. P., Hardisty D. S., Hood A. v. S. and Planavsky N. J. (2017) Investigating controls on boron isotope ratios in shallow marine carbonates. *Earth Planet. Sci. Lett.* **458**, 380–393.

Zhou Y., Fang Y., Fang C., Zhu F., Ge H. and Chen Q. (2013) Solution structure of energy stored system I: aqua-$B(OH)_4^-$: a DFT, Car–Parrinello molecular dynamics, and Raman study. *J. Phys. Chem. B* **117**, 11709–11718.

Associate editor: Edwin Schauble